Environmental and vegetational changes recorded in sedimentary leaf wax n-alkanes across the Cretaceous-Paleogene boundary at Loma Capiro, Central Cuba

Environmental and vegetational changes recorded in sedimentary leaf wax *n*-alkanes across the Cretaceous–Paleogene boundary at Loma Capiro, Central Cuba

Shinya Yamamoto[a,*], Takashi Hasegawa[a], Ryuji Tada[b], Kazuhisa Goto[c,1], Reinaldo Rojas-Consuegra[d], Consuelo Díaz-Otero[e], Dora E. García-Delgado[f], Shinji Yamamoto[b], Hironobu Sakuma[b], Takafumi Matsui[g,1]

[a] *Department of Earth Sciences, Graduate School of Natural Science and Technology, Kanazawa University, Kakuma, Kanazawa 920-1192, Japan*

[b] *Department of Earth and Planetary Science, Graduate School of Science, The University of Tokyo, 7-3-1 Hongo, Tokyo 113-0033, Japan*

[c] *Disaster Control Research Center, Graduate School of Engineering, Tohoku University, Aoba 06-6-11, Aramaki, Sendai 980-8579, Japan*

[d] *Museo Nacional de Historia Natural, Obispo No. 61, Plaza de Armas, La Habana Vieja 10100, Cuba*

[e] *Instituto de Geología y Paleontología Vía Blanca y Línea del Ferrocarril. San Miguel del Padrón, La Habana 11 000, Cuba*

[f] *Centro de Investigaciones del Petróleo, Washington No. 166, esquina Churruca, Municipio Cerro, Ciudad de la Habana, Cuba*

[g] *Department of Complexity Science and Engineering, Graduate School of Frontier Science, The University of Tokyo, 7-3-1 Hongo, Tokyo 113-0033, Japan*

* Corresponding author. Present address: Institute of Low Temperature Science, Hokkaido University, N19W8, Kita-ku, Sapporo 060-0819, Japan. Fax: +81-11-706-7142.

E-mail address: s.yamamoto@pop.lowtem.hokudai.ac.jp (S. Yamamoto)

[1] Present address: Planetary Exploration Research Center, Chiba Institute of Technology, 2-17-1 Tsudanuma, Narashino 275-0016, Chiba, Japan.

ABSTRACT

The stable carbon isotopic compositions ($\delta^{13}C$) and chain-length distribution [ACL and $n\text{-}C_{31}/(n\text{-}C_{29}+n\text{-}C_{31})$] of sedimentary leaf wax *n*-alkanes were investigated across the Cretaceous–Paleogene (K–Pg) boundary at Loma Capiro, Central Cuba, to reconstruct paleoenvironmental changes that are recorded in terrestrial higher plants. The stratigraphic profiles of the *n*-alkane $\delta^{13}C$ values show a negative excursion in the lowermost Paleocene, although its magnitude is much smaller (~0.3‰) than the global signals (1.5 to 2.0‰) in the surface ocean-atmospheric carbon reservoir. Relations between the *n*-alkane $\delta^{13}C$ values and the $C_{31}/(C_{29} + C_{31})$ ratios exhibit two different trends, suggesting that our $\delta^{13}C$ records are likely affected by two types of paleoenvironmental factors in addition to the $\delta^{13}C$ variations in the exogenous carbon reservoir. Rare occurrence of terrigenous organic matter that is usually transported by rivers suggests that the *n*-alkanes at Loma Capiro are likely to have been transported by trade winds, which recorded paleoenvironmental conditions of the northwestern part of the African continent. The *n*-alkane $\delta^{13}C$ values show a parallel decrease with the ACL and $C_{31}/(C_{29} + C_{31})$ values in the first 37,000 yrs following the K–Pg boundary. Such decreases are consistent with plant physiological responses to reduced net evaporation, suggesting a possible influence of the impact-induced warm-humid condition in the early Paleocene. In contrast, the *n*-alkane $\delta^{13}C$ values are negatively correlated with the $C_{31}/(C_{29} + C_{31})$ ratios from 40,000 to 67,000 yrs after the K–Pg boundary. This time period matches well with that required for the recovery of terrestrial floras from the K–Pg mass extinction to those with diversity equivalent to the late Cretaceous, suggesting that the *n*-alkane signals are also likely affected by the plant diversification

process after the mass extinction.

Keywords: K–Pg boundary, Cretaceous, Paleogene, stable carbon isotopes, *n*-alkane, leaf wax

1. Introduction

The mass extinction event at the Cretaceous–Paleogene (K–Pg) boundary is one of the five largest mass extinction events in the Phanerozoic. More than 15% of fossil families went extinct in the ocean (Raup and Sepkoski, 1982), and 15% to 57% of diverse Cretaceous flora abruptly disappeared on land (Orth et al., 1981; Wolfe and Upchurch, 1987; Johnson et al., 1989; Vajda and Raine, 2003; Wilf and Johnson, 2004; Nichols, 2007). The stable carbon isotopic compositions ($\delta^{13}C$) of the surface ocean (e.g. Hsü et al., 1982; Gilmour et al., 1987; Keller and Lindinger, 1989; Meyers and Simoneit, 1990; Meyers, 1992; Hollander et al., 1993) and terrestrial sedimentary carbon (Schimmelmann and DeNiro, 1984; Arinobu et al., 1999; Arens and Jahren, 2000, 2002) show an abrupt negative excursion at the K–Pg boundary, suggesting a large impact of this mass extinction on global carbon cycles. Combined stratigraphical, micropaleontological, petrological and geochemical data show that this mass extinction was triggered by a large asteroid impact at Chicxulub on Yucatan peninsula, Mexico (Schulte et al., 2010).

The $\delta^{13}C$ values of terrestrial higher plants are primarily controlled by the isotopic composition of atmospheric CO_2 (Farquhar et al., 1982; Arens et al., 2000). Therefore, stratigraphic records of plant $\delta^{13}C$ values can provide good constraints on the rate and magnitude of disruption in the global carbon cycles. The $\delta^{13}C$ excursion in sedimentary leaf wax *n*-alkanes implies a loss of at most 24% of the Cretaceous biomass at the boundary (Arinobu et al., 1999).

On the other hand, the $\delta^{13}C$ values of terrestrial higher plants are also sensitive to isotopic fractionations that reflect ecological and physiological responses to their growing environment (Farquhar et al., 1989; Arens et al., 2000), as well as taxonomic variations within contributing plant communities (Arens and Jahren, 2002). Because abundant evidences suggest a global turnover in vegetation (Vajda and Raine, 2003) and changes in continental climate (Wolfe and Upchurch, 1987; Wolfe, 1990; Lehman, 1990) at the K–Pg boundary, these changes might have affected the $\delta^{13}C$ values of terrestrial higher plants. In fact, the magnitudes of the $\delta^{13}C$ excursions recorded in terrigenous organic matter across the K–Pg boundary range from –1.1 to –2.8‰ (Arinobu et al., 1999; Arens and Jahren, 2000, 2002), exhibiting much larger variations than those caused by the plant vital effects (~0.8‰; Arens and Jahren, 2002). However, the causes for these $\delta^{13}C$ variations still remain unclear.

Several studies have shown that comparison of the $\delta^{13}C$ fluctuations of terrigenous organic matter with those in the exogenous carbon reservoir, such as marine carbonate, is useful to reconstruct paleoenvironmental signals that are recorded in terrestrial higher plants (e.g. Hasegawa et al., 2003). However, this approach cannot be utilized for K–Pg boundary sequences because the shape and magnitude of the $\delta^{13}C$ changes of marine carbonates are also affected by changes in calcareous microfossil compositions, size distributions of planktonic foraminiferal species, and local productivity (D'Hondt and Zachos, 1993; Barrera and Keller, 1994).

Long chain (C_{27} to C_{33}) *n*-alkanes with an odd/even carbon number predominance are typical of terrestrial higher plant waxes (Eglinton and Hamilton, 1967). These *n*-alkanes are ubiquitous in marine sediments (Pancost and Boot, 2004), and their chain-length distributions are sensitive to changes in the plant growing environment and the composition of their source vegetation (Hall and Jones, 1961; Poynter et al., 1989; Schefuß et al., 2003; Sachse et al., 2006). Hence, we assess

paleoenvironmental conditions that may have been recorded in terrestrial higher plants using two *n*-alkane biomarker proxies based on their chain length distribution, i.e., the average chain length (ACL_{27-33}) and the $C_{31}/(C_{29} + C_{31})$ ratio. The ACL_{27-33} is the concentration-weighted mean chain length of the C_{27} to C_{33} odd carbon number *n*-alkanes (Poynter et al., 1989), and its variations are generally related to environmental changes such as the temperature and aridity in which their source vegetation grows (Gagosian and Peltzer, 1986; Poynter et al., 1989; Schefuβ et al., 2003; Rommerskirchen et al., 2003). In contrast, the $C_{31}/(C_{29} + C_{31})$ ratio is the concentration ratio of the C_{31} *n*-alkanes to the sum of the C_{29} and C_{31} *n*-alkanes (Schefuβ et al., 2003), and its variations are more closely related to changes in aridity, than in temperature and vegetation type (Schefuβ et al., 2003).

The ultimate objective of this study is to reconstruct the environmental and vegetational changes that may be recorded in the $\delta^{13}C$ variations across the K–Pg boundary. Here we report the results from the hemipelagic K–Pg sequence at Loma Capiro, central Cuba, in which a published planktonic foraminiferal biostratigraphy (Alegret et al., 2005) and a high sedimentation rate allow us to conduct a stratigraphically well-constrained, high-resolution analysis of this boundary sequence.

2. Setting and stratigraphy of Loma Capiro

Loma Capiro is a small hill of ca. 180 m height in the northeast part of the Santa Clara city, central Cuba (Fig. 1), that provides an excellent exposure of the K–Pg boundary sequence on its southern slope. The K–Pg boundary sequence at Loma Capiro is composed of a hemipelagic sequence of foraminifera-rich massive gray calcareous mudstone and sandstone, and a 10.9 m-thick clastic complex (Fig. 2). These sediments are included in the upper Maastrichtian Santa Clara Formation and the Paleocene Ochoa Formation (Rojas-Consuegra et al., 2007). Paleogeographic reconstructions suggest that

129 the K–Pg location of the site was about 500 km south of its present position and that its
130 sediment accumulated on the northeastern slope of the Cuban carbonate platform on the
131 south edge of the proto-Caribbean Basin (Fig. 1d; Rojas-Consuegra et al., 2005;
132 Núñez-Cambra and Rojas-Consuegra, 2007; Goto et al., 2008). Benthic foraminiferal
133 assemblages indicate a paleodepth of 700 m to 3,000 m (Alegret et al., 2005).
134 The lithology of uppermost 1.5 m of the Maastrichtian is marked by
135 well-lithified gray calcareous mudstone followed by a continuous upward-fining
136 sequence of the clastic complex with an erosional contact (Fig. 2). The basal 6.5 m of
137 the sequence is characterized by a matrix-supported breccia with siltstone to very fine
138 sandstone matrix and rounded clasts of mudstone, limestone, gabbro and serpentinite.
139 Diameters of these clasts are generally less than 10 cm. Neither imbrication nor changes
140 in grain size are observed. The subsequent 1.5 m of the sequence is upward-fining
141 microbreccia with cross lamination, which is overlain by 65 cm-thick medium to coarse
142 sandstones. The uppermost 2.5 m of the complex is composed of an upward-fining
143 sequence of coarse-medium to medium-fine sandstones with intercalations of 15
144 cm-thick limestone and 10 cm-thick whitish clay layers.
145 Similar end-Cretaceous clastic deposits have been widely recognized around
146 the Gulf of Mexico and in the proto-Caribbean Sea (Smit et al., 1996; Tada et al., 2003;
147 Schulte et al., 2006; Goto et al., 2008). Lithologic and paleontologic evidence suggests
148 that these sediments were deposited in a geologically instantaneous period by the
149 collapse of carbonate platforms, gravity flows and large tsunamis that are associated
150 with the K–Pg impact at Chicxulub (Bralower et al., 1998). Likewise, the presence of
151 reworked Cretaceous foraminifera and impact materials in the clastic complex at Loma
152 Capiro suggests its link to the K–Pg impact (Alegret et al., 2005). We therefore placed
153 the K–Pg boundary at the bottom of the clastic complex (= basal 0 in Fig. 2).
154 The boundary between the clastic complex and the Paleocene mudstone is

sharp and marked by light to dark gray mudstone that has a strike of N75°E and a northward dip of 56° (Fig. 1c). The lower half of the Paleocene sequence is mainly composed of light gray to brownish gray mudstone with intercalations of sandstone layers. In contrast, the upper half of the sequence is generally characterized by alternating beds of light gray to reddish brown mudstone and 1 to 15 cm-thick light gray fine to medium sandstone. An intercalation of ca. 50 cm-thick fine to medium sandstone is observed at the 454 cm horizon above the clastic complex (Fig. 2).

Three planktonic foraminiferal datums are assigned to the 200 cm, 248.7 cm and 520 to 620 cm horizons above the clastic complex by comparison to the results of Alegret et al. (2005) (Fig. 2). The ages of these datums are 64.9 Ma, 64.5 Ma and 63.0 Ma, respectively (Berggren et al., 1995). Linear sedimentation rates (LSR) of the Paleocene sequence above the clastic complex are therefore calculated as 2.0 cm/kyr for the 0–200 cm, 0.1 cm/kyr for the 200–248.7 cm, and 0.2 cm/kyr for the 248.7–620 cm interval.

3. Materials and Methods

3.1. Samples

Samples were obtained from the upper 1.5 m of the Maastrichtian calcareous mudstone and the lower 11 m of the Paleocene mudstone above the clastic complex (Fig. 2). We did not collect samples from the complex because it is mainly composed of reworked Cretaceous materials that the impact left behind, and therefore we put a 0 horizon for the Paleocene sequence at the top of the clastic complex (= top 0 in Fig. 2). We used two slightly separated transects for sampling because the vertical exposure that contained the Maastrichtian section did not allow collection of stratigraphically continuous Paleocene samples. Both transects are well correlated by the upper boundary

of the clastic complex. The outcrop was trenched to about 1 m to obtain fresh unweathered samples. Sampling resolutions that are estimated from the LSRs of the Paleocene range from several thousand years to several hundreds of thousand years.

3.2. Measurements of calcium carbonate ($CaCO_3$) and total organic carbon (TOC) concentrations

Powdered samples were treated with 5N-HCl for 24h to remove carbonate minerals. Subsequently, the sediments were rinsed with deionized water to remove $CaCl_2$ and dried in an oven (60 °C). The concentrations of calcium carbonate were calculated using weight differences before and after the acid treatment. Measurements of total organic carbon (TOC) content were performed on a Thermo Finnigan FlashEA 1112 elemental analyzer at the Center for Marine Core Research, Kochi University.

3.3. Organic geochemical analysis

3.3.1. Extraction and separation

The samples were powdered in an agate mill after removal of surface contaminants and drying in an oven (60 °C) overnight. Finely ground samples (ca. 25−120 g) were Soxhlet extracted with CH_2Cl_2 (DCM) for 48 h. The extracts were separated into aliphatic, aromatic, ketone and polar fractions using silica gel column chromatography (5% H_2O deactivated) by elution with *n*-hexane (2 ml), *n*-hexane/DCM (3:1, v/v, 3 ml), DCM (3 ml) and DCM/MeOH (4:1, v/v, 4 ml), respectively. Blank tests showed that there was no laboratory contamination of *n*-alkanes during the procedure. These lipid fractions were analyzed using gas chromatography (GC) and GC/mass spectrometry (MS) at Kanazawa University. For compound-specific stable carbon isotope analyses, sufficient amounts of *n*-alkanes were purified using the urea adduction technique (Hasegawa et al., 2006) and then determined by GC/isotope ratio monitoring

MS (GC/irmMS) at the Center for Marine Core Research, Kochi University.

3.3.2. GC and GC/MS

GC analysis was performed using a Hewlett-Packard 6890 gas chromatograph equipped with an on-column injector, an HP-1 fused silica capillary column (30 m × 0.32 mm i.d., 0.25 μm film thickness) connected with 5 m guard column and a flame ionization detector (FID). Helium was used as the carrier gas. The GC oven temperature was programmed from 50 °C to 120 °C at 30 °C/min, then to 310 °C at 5 °C/min and held isothermally for 19.57 min. GC/MS analysis was performed using a Hewlett-Packard 5973 Mass Selective Detector coupled to a Hewlett-Packard 6890 GC equipped with a HP-5MS fused silica capillary column (30 m × 0.25 mm i.d., 0.25 μm film thickness) and split/splitless injector. The temperature program was the same as for GC analysis. The MS was operated in Electron-Impact mode at 70 eV, scanning a mass range of *m/z* 40-650 at 2.44 scans per second. The compounds were identified on the basis of their mass spectra, GC retention times, and comparison with literature spectra.

3.3.3. Compound-specific carbon isotope analysis

$^{13}C/^{12}C$ ratios of individual *n*-alkanes were determined using a Finnigan MAT Delta ^{plus} XP mass spectrometer interfaced with a Trace GC, via a combustion furnace maintained at 840 °C. The GC was equipped with a HP-5MS fused silica capillary column (30 m × 0.32 mm i.d., 0.25 μm film thickness) and split/splitless injector. Helium was used as the carrier gas. The GC oven was ramped from 50 °C to 310 °C at 4 °C/min and held isothermally for 25 min. CO_2 gas with a pre-calibrated isotopic composition was used as a standard. The $\delta^{13}C$ values are expressed as per mil (‰) relative to the Vienna Pee Dee Belemnite (VPDB). A standard mixture consisting of C_{16} to C_{30} *n*-alkanes of known isotopic values was daily injected into the system to check the data quality and to ensure the analytical error to be ±0.5‰. Reported isotopic data

represent an averaged value of the multiple analyses.

3.4. Organic petrological examination

Crushed mudstone was prepared into polished blocks following the standard preparation procedure described in Bustin et al. (1983). Observation of organic particles was performed using a MPV-2 microscope.

4. Results

4.1. $CaCO_3$ and TOC concentrations

$CaCO_3$ concentrations in the Cretaceous samples range from 42.7% to 56.4%, whereas those in the Paleocene range from 14.2% to 61.8% (Fig. 2). The concentration drops to 25.4% at the top 0 horizon and stays low until LC-A-113.1. The concentration increases to 53.3% at LC-A-129.7 and fluctuates between 22.6% and 61.8% for the rest of the section (Fig. 2). TOC concentrations are extremely low (0.01% to 0.05%) throughout the sequence and do not show any significant stratigraphic variation (Fig. 2).

4.2. Extractable organic compounds

Aliphatic hydrocarbon fractions are mainly composed of terrestrial higher plant-derived long chain (C_{27} to C_{33}) *n*-alkanes. These *n*-alkanes are characterized by a strong odd/even carbon number predominance (Fig. 3), as evidenced by high carbon preference index ($CPI_{29\text{-}33}$) values of 3.7 to 6.0 for the upper Cretaceous samples and 1.8 to 7.4 for the Paleocene samples (Fig. 4). The concentrations of C_{29} and C_{31} *n*-alkanes range from 0.4 to 39.0 ng/g dry sediment and 0.5 to 46.4 ng/g dry sediment, respectively (Fig. 4). The C_{31} *n*-alkane is found as the most abundant homologue except for samples LC-A-29.2 and LC-C-34.5 in which the C_{29} *n*-alkane dominates. The

occurrence of resin-derived higher plant biomarkers, i.e., aromatic terpenoids, is rare, and higher plant-derived *n*-fatty acids and alcohols are not detected.

4.3. Stratigraphic fluctuations in the $\delta^{13}C$, ACL, and $C_{31}/(C_{29} + C_{31})$ values of n-alkanes

Fig. 4 shows the stratigraphic fluctuations of stable carbon isotopic compositions ($\delta^{13}C$), average chain length ($ACL_{27\text{-}33}$) and $C_{31}/(C_{29} + C_{31})$ ratio of *n*-alkanes. The $\delta^{13}C$ values of the C_{29} *n*-alkane range from –28.8‰ to –27.8‰, whereas those of the C_{31} *n*-alkanes range from –29.7‰ to –28.6‰. The $\delta^{13}C$ values of the C_{31} *n*-alkane are found to be more depleted in ^{13}C by up to 1.2‰ compared to the C_{29} *n*-alkane throughout the section. The ACL and the $C_{31}/(C_{29} + C_{31})$ ratio range from 29.91 to 30.63 and 0.47 to 0.64, respectively. The ACL values are relatively low (29.91 to 30.17) in the lower Paleocene (LC-C-2 to LC-A-79.7), and the other proxies show prominent negative excursions from LC-C-24.5 to LC-A-61.7 with peak values of 0.47 for the $C_{31}/(C_{29} + C_{31})$ ratio (LC-A-29.2) and of –28.8‰ (LC-C-40) and –29.5‰ (LC-C-40, 50) for the $\delta^{13}C$ of the C_{29} and C_{31} *n*-alkanes, respectively.

The stratigraphic profiles of the $\delta^{13}C$, ACL and $C_{31}/(C_{29} + C_{31})$ values enable us to subdivide the section into four distinctive intervals (LC I–IV; Fig. 4). LC I is the upper Cretaceous interval that is characterized by relatively constant values of the $\delta^{13}C$, ACL and $C_{31}/(C_{29} + C_{31})$ ratio. LC II is the first 79.7 cm interval above the clastic complex that is characterized by low ACL values and prominent negative shifts in the $C_{31}/(C_{29} + C_{31})$ and $\delta^{13}C$ values. LC III is the interval between LC-A-79.7 and LC-A-224.7 in which the $\delta^{13}C$ values and the ACL and $C_{31}/(C_{29} + C_{31})$ values vary in opposite directions. LC IV covers the rest of the section, characterized by parallel trends in these three parameters.

4.4. Microscopic observation of organic particles

Organic particles in two Paleocene samples (LC-C-2, LC-A-243.5) are mainly composed of terrestrially derived tiny (<10 μm) vitrinite fragments. The occurrence of these organic particles is rare, and the shapes of the fragments are subrounded to subangular with medium to high reflectance. Organic particles derived from marine organisms were not detected.

5. Discussion

5.1. Transportation mechanism of terrestrial higher plant-derived n-alkanes

Terrestrially derived organic matter is generally transported to marine sediments by winds and fluvial processes (De Leeuw et al., 1995). The location of Loma Capiro was more than 500 km south of its present position at the time of the K–Pg event (Tada et al., 2003; Goto et al., 2008), and thus riverine delivery of organic matter from the North American continent is unlikely due to the long transport distance (>1,000 km; Fig. 1d). However, contributions from the nearby Cuban arc complex could have occurred.

Because rivers can transport large quantities of particulate and dissolved organic carbon from the continents (Hedges et al., 1997), sediments deposited near rivers are expected to contain a significant amount of terrestrial organic matter. However, the occurrence of higher plant derived particulate organic matter at Loma Capiro is rare (See *4.4*). In addition, low concentrations of resin-derived organic compounds that are usually transported by rivers (Simoneit, 1977) such as retene suggest that the riverine transport of terrigenous organic compounds had also been not very significant at Loma Capiro.

According to model simulations of late Cretaceous atmospheric circulation, the proto-Caribbean sedimentary basin was under the influence of the Northeast trade

298 winds (Cousin-Rittemard et al., 2002). Hence, the terrestrial higher plant-derived
299 *n*-alkanes at Loma Capiro are most likely to have been long-range transported via the
300 trade winds.

301 *5.2. Stratigraphic fluctuations of the n-alkane $\delta^{13}C$ values across the K–Pg boundary*

302 The $\delta^{13}C$ of terrestrial higher plants is primarily controlled by that in
303 atmospheric CO_2 (Farquhar et al., 1982; Arens et al., 2000). However, our $\delta^{13}C$ profiles
304 of terrestrial higher plant-derived *n*-alkanes exhibit only a weak negative shift (~0.3‰)
305 in the lowermost Paleocene (LC II; Fig. 4), compared to the globally synchronous 1.5 to
306 2.0‰ negative excursion observed in the surface ocean-atmospheric carbon reservoir
307 (e.g. Hsü et al., 1982; Zachos and Arthur, 1986; Keller and Lindinger, 1989; Arinobu et
308 al., 1999; Arens and Jahren, 2000; 2002).
309 Similarly diminished excursions at the boundary have been reported in the
310 $\delta^{13}C$ values of bulk organic matter from Dogie Creek, Montana (Maruoka et al., 2007)
311 and Stevns Klint, Denmark (Brisman et al., 2001). These studies attributed such a small
312 shape of the excursions to an increased input of ^{13}C-enriched organic materials from
313 algae and wildfires. However, *n*-alkane contributions from these sources are not likely
314 to have occurred at Loma Capiro because relatively high CPI values of the *n*-alkanes
315 suggest that they originated exclusively from terrestrial higher plant waxes. In addition,
316 although the TOC concentrations of our samples are extremely low, a contamination
317 from contemporary plant sources is very unlikely because of the absence of long chain
318 *n*-fatty acids and alcohols, main constituents of contemporary plant leaf waxes as along
319 with the *n*-alkanes (Eglinton and Hamilton, 1967).
320 In general, there is a large input of ancient plant materials from soil to marine
321 sediments (Eglinton et al., 1997; Matsumoto et al., 2001). Thus, enhanced delivery of
322 these materials could have concealed the global ^{13}C-enriched signal. However, a marked

change in the *n*-alkane distributions before and after the K–Pg boundary (Fig. 3) indicates a systematic change in their plant sources. Further, the averaged time lag in delivery of soil organic matter (12,000 yrs; Eglinton et al., 1997; Matsumoto et al., 2001) is too short to dilute the signal of the globally synchronous excursion spanning more than several tens of thousands years (Arinobu et al., 1999; Arens and Jahren, 2000; Therrien et al., 2007).

Our lowermost Paleocene sample (LC-C-2) represents sediments that deposited within the first 20,000 yrs following the K–Pg boundary (Alegret et al., 2005) in which the $\delta^{13}C$ of terrestrial organic matter shows the globally synchronous excursion. Thus, the $\delta^{13}C$ values of the *n*-alkanes at Loma Capiro should exhibit a 1.5 to 2.0‰ negative excursion in LC II if they reflected the global $\delta^{13}C$ signal. The absence of such excursion suggests that our $\delta^{13}C$ records are likely affected by factors other than the $\delta^{13}C$ variations in the exogenous carbon reservoir.

5.3. Factors controlling the n-alkane $\delta^{13}C$ values at Loma Capiro

The stable carbon isotopic compositions ($\delta^{13}C$) of terrestrial higher plants are sensitive to photosynthetic carbon fixation pathways and isotopic fractionations that reflect physiological responses to conditions in their growing environment, such as continental aridity, light level, and growing temperature (Farquhar et al., 1982; Arens et al., 2000), as well as taxonomic variations in contributing plant communities (Arens et al., 2000; Chikaraishi and Naraoka, 2003). However, *n*-alkane contribution from C_4 plants is very unlikely at the time of the K–Pg boundary because the expansion of C_4 grass-dominated savannah did not occur until the Middle to Late Miocene (Jacobs et al., 1999). Lower $\delta^{13}C$ values in C_{31} *n*-alkane as compared with C_{29} also suggest that the *n*-alkanes unlikely originated from C_4 plants in which *n*-alkanes usually show nearly constant isotopic composition across their different chain lengths (–17‰ to –24‰;

348 Collister et al., 1994; Kuypers et al., 1999).

349 In Fig. 5, we show a cross plot of the weighted-mean $\delta^{13}C$ values of the C_{29}
350 and C_{31} *n*-alkanes ($\delta^{13}C_{WM}$) and the $C_{31}/(C_{29} + C_{31})$ ratios from the four stratigraphic
351 intervals (LC I to IV). Although the correlations are not significant in LC I and LC IV,
352 the $\delta^{13}C_{WM}$ and the $C_{31}/(C_{29} + C_{31})$ values are positively correlated in LC II ($r = 0.89$; $p =$
353 0.04), whereas in LC III negatively correlated ($r = 0.91$; $p < 0.01$) (Fig. 5). Because the
354 chain length distribution of *n*-alkanes are sensitive to changes in the plant growing
355 environment and the composition of their source vegetation (Hall and Jones, 1961;
356 Poynter et al., 1989, Schefuβ et al., 2003; Sachse et al., 2006), the presence of these
357 different trends in the $\delta^{13}C$-$C_{31}/(C_{29} + C_{31})$ diagram suggests that the *n*-alkane $\delta^{13}C$
358 values are controlled by two types of paleoenvironmental factors in addition to the $\delta^{13}C$
359 of the exogenous carbon reservoir.

360 Contemporary observations reveal that important quantities of African dust
361 are carried across the equatorial Atlantic to the Caribbean via the trade winds (Prospero
362 and Lamb, 2003). Hence, the *n*-alkane signals at Loma Capiro likely represent
363 paleoenvironmental conditions of the northwestern part of the African continent
364 reflecting a wide zonal wind regime of the trade winds and a mixing during the
365 long-range transport.

366 *5.4. Environmental control on the n-alkane $\delta^{13}C$ values in the lower Paleocene (LC II)*

367 Several lines of evidence indicate enhanced greenhouse warming at the early
368 Paleocene as a result of the impact-induced CO_2 release from carbonate platforms and
369 the reduction of primary productivity (Hsü et al., 1982; O'Keefe and Ahrens, 1989).
370 Oxygen isotope records in marine carbonates reveal a period of gradual warming of
371 surface waters spanning a few hundred to several hundred thousand years following the
372 K–Pg boundary (Hsü et al., 1982; Zachos et al., 1989; Kaiho et al., 1999). At the same

time, records of plant leaf fossils and clay minerals also give evidence for increased temperature and precipitation on land (Wolfe and Upchurch, 1987; Wolfe, 1990; Kaiho et al., 1999), although a study on paleosols estimates a humid but cool climate in western North America (Lehman, 1990). In the Southern Hemisphere, pollen assemblages in New Zealand suggest transient warm humid conditions (Vajda et al., 2001).

The stratigraphic variations of the $\delta^{13}C$ values show parallel decreases with the ACL and $C_{31}/(C_{29} + C_{31})$ values in LC II (Fig. 4). In terms of plant physiology, such decreases in these *n*-alkane proxies can be interpreted as plant responses to reduced evapotranspiration. This response is because plants can alter the chain-length of leaf waxes to minimize loss of water vapor from their leaves (Sachse et al., 2006). Under a less evaporative condition, plants no longer need to reduce stomatal conductance to conserve water in their leaves, which results in the $\delta^{13}C$ values becoming more ^{13}C depleted (Farquhar et al., 1982). Hence, the concurrent decreases in the ACL and $C_{31}/(C_{29} + C_{31})$ values and the $\delta^{13}C$ values in LC II seem to indicate a less evaporative condition in the early Paleocene.

The age calculation based on the LSR for this interval indicates that the duration of decreases in the $\delta^{13}C$, ACL and $C_{31}/(C_{29} + C_{31})$ values range from 9,700 to 37,000 yrs after the K-Pg boundary. This time period is consistent with that estimated for the impact-induced warming (10^4 to 10^5 years; O'Keefe and Ahrens, 1989), suggesting its relation to this transient warmth, although geochemical evidence indicates that such warmth lasted only for a few thousand years following the boundary (Kaiho et al., 1999). In contrast, the record of dinoflagellate cysts and benthic foraminifera at El Kef, Tunisia, implies a ~2,000 yrs cooling following the K–Pg boundary in association with an impact winter (Galeotti et al., 2004). Relatively high $\delta^{13}C$, ACL and $C_{31}/(C_{29} + C_{31})$ values in our lowermost sample in the Paleocene (LC-C-2) might, thus, have been

399 resulted from plant responses to this cooling.

400 *5.5. Vegetational control on the n-alkane $\delta^{13}C$ values in the lower Paleocene (LC III)*

401 The $C_{31}/(C_{29} + C_{31})$-$\delta^{13}C$ distributions exhibit marked differences between
402 before (LCI) and after (LC II) the K–Pg boundary, but the distribution of LC II
403 gradually shift back to the identical area as in the upper Cretaceous (LC I) through the
404 lower Paleocene (LC III; Fig. 5). Because the LC I and LC III distributions lie away
405 from the regression lines of LC II (Fig. 5), the shifts in the distributions should have
406 been controlled by some factor other than what caused the LC II variations (see *5.4*).
407 In Fig. 6, we showed the stratigraphic profiles of the $C_{31}/(C_{29} + C_{31})$ ratio at
408 Loma Capiro and those in the K–Pg boundary sediments from Far East Asia (Mita and
409 Shimoyama, 1999). Interestingly, both $C_{31}/(C_{29} + C_{31})$ patterns exhibit similar decreases
410 following the K–Pg boundary. Such similarities between the sections that are >10,000
411 km apart indicate that the variations are likely resulted from a globally simultaneous
412 event, i.e., the K–Pg mass extinction.
413 At the K–Pg boundary, 15% to 57% of the late Cretaceous mega and
414 palynofloral species went extinct (e.g. Vajda and Raine, 2003; Wilf and Johnson, 2004;
415 Nichols, 2007). The devastated land flora was for a short period replaced by a fungal
416 community (Vajda and McLoughlin, 2004), which followed by the recovery succession
417 of photosynthetic plants that starts with a fern dominance, the so-called fern spike, in
418 North America, New Zealand and Far East Asia (Tschudy et al., 1984; Vajda et al.,
419 2001; Saito et al., 1986). In contrast, a rise of angiosperm and bryophyte floras are
420 reported in northern Canada and in the Netherlands, respectively (Sweet et al., 1990;
421 Brinkhuis and Schiøler, 1996). Vegetation with a diversity equivalent to that in the late
422 Cretaceous was subsequently established through angiosperm recolonization in North
423 America and tree ferns and gymnosperm dominances in New Zealand (Wolfe and

Upchurch, 1987; Vajda et al., 2001).

Although Méon (1990) concluded that no abrupt extinction occurred in northwestern Africa, palynological data at El Kef, Tunisia, which is close to the possible source area of leaf wax *n*-alkanes at Loma Capiro, show disappearance of 13.6% of the upper Maastrichtian palynoflora at the boundary (Nichols and Johnson, 2008). Because the C_{31} *n*-alkane is generally more abundant in grasses and in certain species of other angiosperms and conifers (Cranwell, 1973; Bi et al., 2005; Sachse et al., 2006; Rommerskirchen et al., 2006), the good negative correlation between the *n*-alkane $\delta^{13}C$ values and the $C_{31}/(C_{29} + C_{31})$ ratios in LC III might be attributed to vegetational changes at the K–Pg boundary. In support for this idea, the $C_{31}/(C_{29} + C_{31})$ variations show good correspondence with an increase of the angiosperm/fern ratios in Far East Asia (Fig. 6). However, there is no corresponding fern spore increase reported in northwest Africa (Ben Abdelkader et al., 1997).

Based on the LSR of 2.0 cm/kyr for the lower Paleocene, the duration of LC III is calculated as 40,000 to 67,000 yrs after the K–Pg boundary. This time period is fairly longer than the time range for the fern dominance in Far East Asia and New Zealand (several thousands of years; Vajda and Raine, 2003). Instead, it is rather close to the duration taken for the recovery of the pre-boundary pollen assemblages in North America (92,600 to 115,800 yrs; Therrien et al., 2007). Although the lack of a palynological record at Loma Capiro does not allow us to assign any taxonomic information, such correspondence in timing suggest that the $\delta^{13}C$ and $C_{31}/(C_{29} + C_{31})$ variations in LC III are likely a consequence of the plant diversification process after the K–Pg mass extinction.

6. Conclusions

The chain-length distribution [ACL and $C_{31}/(C_{29} + C_{31})$ ratio] and stable

carbon isotopic compositions ($\delta^{13}C$) of sedimentary leaf wax *n*-alkanes were investigated across the Cretaceous-Paleogene (K–Pg) boundary at Loma Capiro, Central Cuba, to assess environmental and vegetational changes that are recorded in terrestrial higher plants. The $\delta^{13}C$ profiles of the *n*-alkanes exhibit a negative excursion following the K–Pg boundary. However, the magnitude of the excursion is much smaller (~0.3‰) than the global signals (1.5 to 2.0‰). The relations between the $\delta^{13}C$ and $C_{31}/(C_{29} + C_{31})$ ratios of the *n*-alkanes reveal that two types of paleoenvironmental factors (such as temperature, humidity and vegetation) have affected this diminished $\delta^{13}C$ variation. The *n*-alkanes at Loma Capiro are likely long-range transported by trade winds, and their signals can be interpreted as reflecting paleoenvironmental conditions of the northwestern part of the African continent. The *n*-alkane $\delta^{13}C$ values show a parallel decrease with the ACL and $C_{31}/(C_{29} + C_{31})$ values in the first 37,000 yrs following the K–Pg boundary, suggesting a possible influence of the impact-induced warm-humid climate in the early Paleocene. In contrast, the *n*-alkane $\delta^{13}C$ values are negatively correlated with the $C_{31}/(C_{29} + C_{31})$ ratios between 40,000 to 67,000 yrs after the K–Pg boundary, suggesting that they likely reflect the plant diversification process after the K–Pg mass extinction.

Acknowledgements

We thank the Japanese Society for Promotion of Science for financial support through a Grant-in-Aid for Scientific Research (B) 17403005 (given to T. Matsui). We also thank V. Vajda (Lund Univ., Sweden) and an anonymous reviewer for valuable comments and suggestions. S.Y. expresses his deep appreciation to M. Ikehara (Kochi Univ.) for assistance and organization of analyses at Kochi University and Y. Suzuki (AIST) for kind assistance for the petrographic study of organic matter. M. Kato, T. Kamiya, N. Hasebe, K. Moriya, T. Yamaguchi (Kanazawa Univ.), and E. Tajika (the

Univ. of Tokyo) provided constructive discussions and valuable suggestions, and P.A. Meyers (The Univ. of Michigan) contributed with comments that improved the English. This research was made possible thanks to an agreement between the Department of Earth and Planetary Science, the University of Tokyo and the Museo Nacional de Historia Natural (Agencia del Medio Ambiente) and the Instituto de Geología y Paleontología del Ministerio de Industria Básica de Cuba. The research was also performed under cooperative research program of the Center for Advanced Marine Core Research (CMCR), Kochi University (06A008, 06B007 and 07A020).

References

Alegret, L., Arenillas, I., Arz, J. A., Díaz, C., Grajales-Nishimura, J. M., Meléndez, A., Molina, E., Rojas, R., Soria, A. R., 2005. Cretaceous–Paleogene boundary deposits at Loma Capiro, central Cuba: evidence for the Chicxulub impact. Geology 33, 721–724, doi: 10.1130/G21573.1.

Arenillas, I., Arz, J.A., Molina, E., 2004. A new high-resolution planktic foraminiferal zonation and subzonation for the lower Danian. Lethaia 37, 79–95.

Arens, N. C., Jahren, A. H., 2000. Carbon isotope excursion in atmospheric CO_2 at the Cretaceous–Tertiary boundary: evidence from terrestrial sediments. Palaios 15, 314–322.

Arens, N. C., Jahren, A. H., 2002. Chemostratigraphic correlation of four fossil-bearing sections in southwestern North Dakota. In: Hartman, J. H., Johnson, K. R., Nichols, D. J. (Eds.), The Hell Creek Formation and the Cretaceous–Tertiary boundary in the northern Great Plains: an integrated continental record of the end of the Cretaceous, Geol. Soc. Amer. Boulder, CO, pp. 75–93.

Arens, N. C., Jahren, A. H., Amundson, R., 2000. Can C3 plants faithfully record the carbon isotopic composition of atmospheric carbon dioxide? Paleobiology 26,

137–164.

Arinobu, T., Ishiwatari, R., Kaiho, K., Lamolda, M. A., 1999. Spike of pyrosynthetic polycyclic aromatic hydrocarbons associated with an abrupt decrease in $\delta^{13}C$ of a terrestrial biomarker at the Cretaceous–Tertiary boundary at Caravaca, Spain. Geology 27, 723–726.

Barrera, E., Keller, G., 1994. Productivity across the Cretaceous/Tertiary boundary in high latitudes. Bull. Geol. Soc. Amer. 106, 1254–1266.

Ben Abdelkader, O., Ben Salem, H., Donze, P., Maamouri, A.-L., Méon, H., Robin, É., Rocchia, R., Froget, L., 1997. The K/T stratotype section of El Kef (Tunisia): events and biotic turnovers. GEOBIOS, M.S.n° 21, 235–245.

Berggren, W.A., Kent, D.V., Aubry, M.-P., Hardenbol, J., 1995. Geochronology, time scales and global stratigraphic correlation, SEPM Spec. Pub., no. 54, 392p.

Bi, X., Sheng, G., Liu, X., Li, C., Fu, J., 2005. Molecular and carbon and hydrogen isotopic composition of *n*-alkanes in plant leaf waxes. Org. Geochem. 36, 1405–1417.

Bralower, T.J., Paull, C.K., Leckie, R.M., 1998. The Cretaceous–Tertiary boundary cocktail: Chicxulub impact triggeers margin collapse and extensive sediment gravity flows. Geology 26, 331–334.

Brinkhuis, H., Schiøler, P., 1996. Palynology of the Geulhemmerberg Cretaceous/Tertiary boundary section (Limburg, SE Netherlands). Geologie en Mijnbouw 75, 193–213.

Brisman, K., Engel, M. H., Macko, S. A., 2001. Distribution, stereochemistry, and stable isotope composition of amino acids in K/T boundary sediments. Precam. Res. 106, 59–77.

Bustin, R. M., Cameron, A. R., Grieve, D. A., Kalkreuth, W. D., 1983. Coal petrology, its principles, methods, and applications. Geol. Assoc. Can. Short Course Note

525 3, Geol. Assoc. Can, Victoria.
526 Chikaraishi, Y., Naraoka, H., 2003. Compound-specific δD-δ^{13}C analyses of *n*-alkanes
527 extracted from terrestrial and aquatic plants. Phytochemistry 63, 361–371,
528 doi:10.1016/s0031-9422(02)00749-5.
529 Collister, J. W., Rieley, G., Stern, B., Eglington, G., Fry, B., 1994. Compound-specific
530 δ^{13}C analyses of leaf lipids from plants with differing carbon dioxide
531 metabolisms. Org. Geochem. 21, 619–627.
532 Cousin-Rittemard, N. M. M., Dijkstra, H. A., Zwagers, T., 2002. Was there a
533 wind-driven Tethys circumglobal current in the Late Cretaceous? Earth Planet.
534 Sci. Lett. 203, 741–753.
535 Cranwell, P. A., 1973. Chain length distribution of *n*-alkanes from lake sediments in
536 relation to post-glacial environmental change. Freshw. Biol. 3, 259–265.
537 De Leeuw, J. W., Frewin, N. L., Van Bergen, P. F., Sinnighe Damsté, J. S., Coolinson, M.
538 E., 1995. Organic carbon as a palaeoenvironmental indicator in the marine
539 realm. In: Bosence, D. W. J., Allison, P. A. (Eds.), Marine
540 Palaeoenvironmental Analysis from Fossils, Geol. Soc., London, pp. 43–71.
541 D'Hondt, S., Zachos, J. C., 1993. On stable isotopic variation and earliest Paleocene
542 planktonic foraminifera. Paleoceanography 8, 527–547.
543 Eglinton, G., Hamilton, R. J., 1967. Leaf epicuticular waxes. Science 156, 1322–1335.
544 Eglinton, T. I., Benitez-Nelson, B. C., Pearson, A., McNichol, A. P., Bauer, J. E., Druffel,
545 E. R. M., 1997. Variability in radiocarbon ages of individual organic
546 compounds from marine sediments. Science 277, 796–799.
547 Farquhar, G. D., O'leary, M. H., Berry, J. A., 1982. On the relationship between carbon
548 isotope discrimination and the intercellular carbon dioxide concentration in
549 leaves. Austral. Jour. Plant Physiol. 9, 121–137.
550 Farquhar, G. D., Ehleringer, J. R., Hubick, K. T., 1989. Carbon isotope discrimination

551 and photosynthesis. Annu. Rev. Plant Physiol. Plant Mol. Biol. 40, 503–537.
552 Gagosian, R. G., Peltzer, E. T., 1986. The importance of atmospheric input of terrestrial
553 organic material to deep sea sediments. Org. Geochem. 10, 661–669.
554 Galeotti, S., Brinkhuis, H., Huber, M., 2004. Records of post-Cretaceous–Tertiary
555 boundary millennial-scale cooling from the western Tethys: A smoking gun for
556 the impact-winter hypothesis? Geology 32, 529-532.
557 Gilmour, I., Orth, C. J., Brooks, R. R., 1987. Carbon at a new K–T boundary site in
558 New Zealand. Meteoritics 22, 385–388.
559 Goto, K., Tada, R., Tajika, E., Iturralde-Vinent, M. A., Matsui, T., Yamamoto, S.,
560 Nakano, Y., Oji, T., Kiyokawa, S., García Delgado, D. E., Díaz Otero, C.,
561 Rojas Consuegra, R., 2008. Lateral lithological and compositional variations
562 of the Cretaceous/Tertiary deep-sea tsunami deposits in northwestern Cuba.
563 Cret. Res., 29, 217–236.
564 Hall, D. M., Jones, R. L., 1961. Physiological significance of surface wax on leaves.
565 Nature 191, 95–96.
566 Hasegawa, T., Pratt, L. M., Maeda, H., Shigeta, Y., Okamoto, T., Kase, T. Uemura, K.,
567 2003. Upper Cretaceous stable carbon isotope stratigraphy of terrestrial
568 organic matter from Sakhalin, Russian Far East: proxy for the isotopic
569 composition of paleoatmospheric CO_2. Palaeogeogr. Palaeoclimatol.
570 Palaeoecol. 189, 97–115.
571 Hasegawa, T., Yamamoto, S., Pratt, L. M., 2006. Data report: stable carbon isotope
572 fluctuation of long-chain n-alkanes from Leg 208 Hole 1263A across the
573 Paleocene/Eocene boundary. In: Kroon, D., Zachos, J. C., Richter, C. (Eds.),
574 Proc. ODP, Sci. Results 208, College station, TX (Ocean Drilling Program), pp.
575 1–11. doi: 10.2973/odp.proc.sr.208.202.2006.
576 Hedges, J. I., Keil, R. G., Benner, R., 1997. What happens to terrestrial organic matter

577 in the ocean? Org. Geochem. 27, 195–212.
578 Hollander, D. J., McKenzie, J. A., Hsü, K. J., 1993. Carbon isotope evidence for
579 unusual plankton blooms and fluctuations of surface water CO_2 in
580 “Strangelove Ocean” after terminal Cretaceous event. Palaeogeogr.
581 Palaeoclimatol. Palaeoecol. 104, 229–237.
582 Hsü, K. J., He, Q., McKenzie, A., Weissert, H., Perch-Nielsen, K., Oberhänsli, H., Kelts,
583 K., LaBrecque, J., Tauxe, L., Krähenbühl, U., Percival, S. F. Jr., Wright, R.,
584 Karpoff, A. M., Petersen, N., Tucker, P., Poore, R. Z., Gombos, A. M.,
585 Pisciotto, K., Carman, M. F. Jr., Schreiber, E., 1982. Mass mortality and its
586 environmental and evolutionary consequences. Science 216, 249–256.
587 Jacobs, B. F., Kingston, J. D., Jacobs, L. L., 1999. The origin of grass-dominated
588 ecosystems. Ann. Missouri Bot. Gard. 86, 590–643.
589 Johnson, K. R., Nichols, D. J., Attrep Jr., M., Orth, C. J., 1989. High-resolution
590 leaf-fossil record spanning the Cretaceous/Tertiary boundary. Nature 340,
591 708–711.
592 Kaiho, K., Kajiwara, Y., Tazaki, K., Ueshima, M., Takeda, N., Kawahata, H., Arinobu,
593 T., Ishiwatari, R., Hirai, A., Lamolda, M. A., 1999. Oceanic primary
594 productivity and dissolved oxygen levels at the Cretaceous/Tertiary boundary:
595 their decrease, subsequent warming, and recovery. Paleoceanography 14,
596 511–524.
597 Keller, G., Lindinger, M., 1989. Stable isotope, TOC and $CaCO_3$ record across the
598 Cretaceous/Tertiary boundary at El Kef, Tunisia. Palaeogeogr. Palaeoclimatol.
599 Palaeoecol. 73, 243–265.
600 Kuypers, M. M. M., Pancost, R. D., Sinninghe Damsté, J. S., 1999. A large and abrupt
601 fall in atmospheric CO_2 concentration during Cretaceous times. Nature 399,
602 342–345.

603 Lehman, T. M., 1990. Paleosols and the Cretaceous/Tertiary transition in the Big Bend
604 region of Texas. Geology 18, 362–364.
605 Maruoka, T., Koeberl, C., Bohor, B. F., 2007. Carbon isotopic compositions of organic
606 matter across continental Cretaceous–Tertiary (K–T) boundary sections:
607 Implications for paleoenvironment after the K–T impact event. Earth Planet.
608 Sci. Lett. 253, 226–238.
609 Matsumoto, K., Kawamura, K., Uchida, M., Shibata, Y., Yoneda, M., 2001. Compound
610 specific radiocarbon and $\delta^{13}C$ measurements of fatty acids in a continental
611 aerosol sample. Geophys. Res. Lett. 28, 4587–4590.
612 Meyers, P. A., 1992. Changes in organic carbon isotope ratios across the K/T boundary:
613 global or local control? In: Macko, S. A., Engel, M. H. (Eds.), Isotope
614 fractionations in organic matter: biosynthetic and diagenetic processes. Chem.
615 Geol. (Isot. Geosci. Sect.) 101, 283–291.
616 Meyers, P. A., Simoneit, B. R. T., 1990. Global comparisons of organic matter in
617 sediments across the Cretaceous/Tertiary boundary. Advances in Organic
618 Geochemistry 1989, Org. Geochem. 16, 641–648.
619 Méon, H., 1990. Palynologic studies of the Cretaceous–Tertiary boundary interval at El
620 Kef outcrop, northwestern Tunisia: Paleogeographic implications. Rev.
621 Palaeobot. Palynol. 65, 85–94.
622 Mita, H., Shimoyama, A., 1999. Characterization of n-alkanes, pristane and phytane in
623 the Cretaceous/Tertiary boundary sediments at Kawaruppu, Hokkaido, Japan.
624 Geochem. Jour. 33, 285–294.
625 Nichols, D. J., 2007. Selected plant microfossil records of the terminal Cretaceous event
626 in terrestrial rocks, western North America. Palaeogeogr. Palaeoclimatol.
627 Palaeoecol. 255, 22–34, doi:10.1016/j.palaeo.2007.02.038.
628 Nichols, D.J., Johnson, K.R., 2008. Plants and the K–T boundary. Cambridge

University Press, New York.

Núñez-Cambra, K., Rojas-Consuegra, R., 2007. Elementos de la estructura de los deslizamientos submarinos en los depósitos del límite K/T en Loma Capiro, Santa Clara, Cuba central. Segunda Convención Cubana de Ciencias de La Tierra, GEOCIENCIA' 2007. Centro Nacional de Información Geológica, IGP, La Habana, pp. 103–104.

O'Keefe, J. D., Ahrens, T. J., 1989. Impact production of CO_2 by the Cretaceous/Tertiary extinction bolide and the resultant heating of the Earth. Nature 338, 247–249.

Orth, C. J., Gilmore, J. S., Knight, J. D., Pillmore, C. L., Tshudy, R. H., Fassett, J. E., 1981. An iridium anomaly at the palynological Cretaceous–Tertiary boundary in northern New Mexico. Science 214, 1341–1343.

Pancost, R. D., Boot, C. S., 2004. The palaeoclimatic utility of terrestrial biomarkers in marine sediments. Mar. Chem. 92, 239–261.

Poynter, J. G., Farrimond, P., Robinson, N., Eglinton, G., 1989. Aeolian-derived higher plant lipids in the marine sedimentary record: links with palaeoclimate. In: Leinen, M., Sarnthein, M. (Eds.), Paleoclimatology and paleometeorology: modern and past patterns of global atmospheric transport, Kluwer Academic Publishers, Dordrecht, The Netherlands, pp. 435–462.

Prospero, J. M., Lamb, P. J., 2003. African droughts and dust transport to the Caribbean: climate change implications. Science 302, 1024–1027, doi:10.1126/science.1089915.

Raup, D. M., Sepkoski, J. J. Jr., 1982. Mass extinctions in the marine fossil record. Science 215, 1501–1503.

Rojas-Consuegra, R., Iturralde-Vinent, M. A., Díaz-Otero, C., García-Delgado, D., Meléndez-Evia, A., Soria, A. R., 2005. Significación paleogeográfica de la

655 brecha basal del Límite K/T en Loma Dos Hermanas (Loma Capiro) en Santa
656 Clara, provincia de Villa Clara. Primera Convención Cubana de Ciencias de la
657 Tierra. Geociencias 8, 1–9.
658 Rojas-Consuegra, R., Díaz-Otero, C., Meléndez, A., Soria, A. R., 2007. Depósito del
659 Límite K–T en Loma Capiro: nueva formación geológica en Cuba central.
660 Segunda Convención Cubana de Ciencias de La Tierra, GEOCIENCIA' 2007.
661 Centro Nacional de Información Geológica, IGP, La Habana, pp. 104–105.
662 Rommerskirchen, F., Eglington, G., Dupont, L., Günter, U., Wenzel, C., Rullkötter, J.,
663 2003. A north to south transect of Holocene southeast Atlantic continental
664 margin sediments: Relationship between aerosol transport and
665 compound-specific $\delta^{13}C$ land plant biomarker and pollen records. Geochem.
666 Geophys. Geosyst. 4(12), 1101, doi:10.1029/2003GC000541.
667 Rommerskirchen, F., Plader, A., Eglinton, G., Chikaraishi, Y., Rullkötter, J., 2006.
668 Chemotaxonomic significance of distribution and stable carbon isotopic
669 composition of long-chain alkanes and alkan-1-ols in C_4 grass waxes. Org.
670 Geochem. 37, 1303–1332.
671 Sachse, D., Radke, J., Gleixner, D., 2006. δD values of individual *n*-alkanes from
672 terrestrial plants along a climatic gradient – implications for the sedimentary
673 biomarker record. Org. Geochem. 37, 469–483.
674 Saito, T., Yamanoi, T., Kaiho, K., 1986. End-Cretaceous devastation of terrestrial flora
675 in the boreal Far East. Nature 323, 253–255.
676 Schefuβ, E., Ratmeyer, V., Stuut, J.-B. W., Jansen, J. H. F., Sinninghe Damsté, J. S.,
677 2003. Carbon isotope analysis of *n*-alkanes in dust from the lower atmosphere
678 over the central eastern Atlantic. Geochim. Cosmochim. Acta 67, 1757–1767.
679 Schimmelmann, A., Deniro, M. J., 1984. Elemental and stable isotope variations of
680 organic matter from a terrestrial sequence containing the Cretaceous/Tertiary

681 boundary at York Canyon, New Mexico. Earth Planet. Sci. Lett. 68, 392–398.
682 Schulte, P., Speijer, R., Mai, H., Kontny, A., 2006. The Cretaceous–Paleogene (K–P)
683 boundary at Brazos, Texas: sequence stratigraphy, depositional events and the
684 Chicxulub impact. Sediment. Geol. 184, 77–109.
685 Schulte, P., Alegret, L., Arenillas, I., Arz, J.A., Barton, P.J., Bown, P.R., Bralower, T.J.,
686 Christeson, G.L., Claeys, P., Cockell, C.S., Collins, G.S., Deutsch, A., Goldin,
687 T.J., Goto, K., Grajales-Nishimura, J.-M., Grieve, R.A.F., Gulick, S.P.S.,
688 Johnson, K.R., Kiessling, W., Koeberl, C., Kring, D.A., MacLeod, K.G.,
689 Matsui, T., Melosh, J., Montanari, A., Morgan, J.V., Neal, C.R., Nichols, D.J.,
690 Norris, R.D., Pierazzo, E., Ravizza, G., Rebolledo-Vieyra, M., Reimold, W.U.,
691 Robin, E., Salge, T., Speijer, R.P., Sweet, A.R., Urrutia-Fucugauchi, J., Vajda,
692 V., Whalen, M.T., Willumsen, P.S., 2010. The Chicxulub Asteroid Impact and
693 Mass Extinction at the Cretaceous-Paleogene Boundary. Science 327,
694 1214–1218.
695 Simoneit, B.R.T., 1977. Diterpenoid compounds and other lipids in deep-sea sediments
696 and their geochemical significance. Geochim. Cosmochim. Acta 41, 463–476.
697 Smit, J., 1982. Extinction and evolution of planktonic foraminifera after a major impact
698 at the Cretaceous/Tertiary boundary. Geol. Soc. Am. Spec. Pap. 190, 329–352.
699 Smit, J., Roep, T.B., Alvarez, W., Montanari, A., Claeys, P., Grajales-Nishimura, J.M.,
700 Bermudez, J., 1996. Coarse-grained, clastic sandstone complex at the K/T
701 boundary around the Gulf of Mexico: Deposition by tsunami waves induced
702 by the Chicxulub impact? In: Ryder, G., Fastovsky, D., Gartner, S. (Eds.), The
703 Cretaceous–Tertiary event and other catastrophes in Earth history. Geol. Soc.
704 America, Boulder, CO, pp. 151–182
705 Sweet, R., Braman, D. R., Lerbekmo, J. F., 1990. Palynofloral response to K/T
706 boundary events: a transitory interruption within a dynamic system.

In: Sharpton, V. L., Ward, P. D. (Eds.), Global Catastrophes in Earth History: an Interdisciplinary Conference on Impacts, Volcanism, and Mass Mortality. Geol. Soc. America, Boulder, CO, pp. 457–469.

Tada, R., Iturralde-Vinent, M. A., Matsui, T., Tajika, E., Oji, T., Goto, K., Nakano, Y., Takayama, H., Yamamoto, S., Kiyokawa, S., Toyoda, K., García-Delgado, D., Díaz-Otero, C., Rojas-Consuegra, R., 2003. K/T boundary deposits in the paleo-western Caribbean basin. In: Bartolini, C., Buffler, R. T., Blickwede, J. (Eds.), The Circum-Gulf of Mexico and the Caribbean: Hydrocarbon habitats, basin formation, and plate tectonics, AAPG Memoir 79, pp. 582–604.

Therrien, F., Eberth, D. A., Braman, D. R., Zelenitsky, D. K., 2007. High-resolution organic carbon isotope record across the Cretaceous–Tertiary boundary in south-central Alberta: implications for the post-impact recovery rate of terrestrial ecosystems and use of $\delta^{13}C$ as a boundary marker. Can. Jour. Earth Sci. 44, 529–542.

Tschudy, R. H., Pillmore, C. L., Orth, C. J., Gilmore, J. S., Knight, J. D., 1984. Disruption of the terrestrial plant ecosystem at the Cretaceous–Tertiary boundary, Western Interior. Science 225, 1030–1032.

Vajda, V., Raine, J. I., 2003. Pollen and spores in marine Cretaceous/Tertiary boundary sediments at mid-Waipara River, North Canterbury, New Zealand. New Zealand Jour. Geol. Geophys. 46, 255–273.

Vajda, V., MacLoughlin, S., 2004. Fungal proliferation at the Cretaceous–Tertiary Boundary. Science 303, 1489.

Vajda, V., Raine, J. I., Hollis, C. J., 2001. Indication of global deforestation at the Cretaceous–Tertiary boundary by New Zealand fern spike. Science 294, 1700–1702.

Wilf, P., Johnson, K. R., 2004. Land plant extinction at the end of the Cretaceous: a

733 quantitative analysis of the North Dakota megafloral record. Paleobiology 30,
734 347–368.
735 Wolfe, J. A., 1990. Palaeobotanical evidence for a marked temperature increase
736 following the Cretaceous/Tertiary boundary. Nature 343, 153–156.
737 Wolfe, J. A., Upchurch, G. R. Jr., 1987. Leaf assemblages across the
738 Cretaceous–Tertiary boundary in the Raton Basin, New Mexico and Colorado.
739 Proc. Natl. Acad. Sci. USA 84, 5096–5100.
740 Zachos, J. C., Arthur, M. A., 1986. Paleoceanography of the Cretaceous/Tertiary
741 boundary event: inferences from stable isotopic and other data.
742 Paleoceanography 1, 5–26.
743 Zachos, J. C., Arthur, M. A., Dean, W. E., 1989. Geochemical evidence for suppression
744 of pelagic marine productivity at the Cretaceous/Tertiary boundary. Nature 337,
745 61–64.

746 **Figure captions**

747 **Fig. 1.** Map showing the location of (a) Santa Clara, (b) Loma Capiro, (c) distribution
748 of the exposure at Loma Capiro, (d) paleogeotectonic setting of Loma Capiro at the
749 Cretaceous–Paleogene boundary (modified after Goto et al., 2008).

750 **Fig. 2.** Stratigraphy, lithology, samples and bulk geochemistry (calcium carbonate and
751 total organic carbon content) of the Cretaceous–Paleogene section at Loma Capiro.
752 *adapted from Alegret et al. (2005). Abbreviation: Cret.; Cretaceous, *A. maya*.;
753 *Abathomphalus mayaroensis Zone*. Note the change in scale due to the presence of a
754 clastic complex at the base of the Paleogene.

755 **Fig. 3.** Gas chromatograms of aliphatic hydrocarbon fraction obtained from (a)
756 Cretaceous and (b) Paleogene samples. Numbers on the GC peaks indicate the
757 carbon chain length of *n*-alkanes. The carbon preference index (CPI) values are also
758 displayed.

759 **Fig. 4.** Stratigraphic profiles of (a) concentration, (b) carbon preference index (CPI), (c)
760 stable carbon isotope ratios ($\delta^{13}C$), (d) $C_{31}/(C_{29} + C_{31})$ ratio and (e) average chain
761 length (ACL) of leaf wax *n*-alkanes in the sediments, which can be separated into
762 four distinctive intervals (LC I to LC IV). For legend and abbreviations, refer Fig. 2.

763 **Fig. 5.** Cross-plot of the weighted-mean $\delta^{13}C$ of C_{29} and C_{31} *n*- alkanes ($\delta^{13}C_{WM}$) versus
764 *n*-C_{31}/(*n*-C_{29}+*n*-C_{31}) ratio. Although relations are not significant in LC I and IV, the
765 $\delta^{13}C_{WM}$ and $C_{31}/(C_{29} + C_{31})$ values are positively correlated in LC II ($r = 0.89$; $p = 0.04$), and are negatively correlated in LC III ($r = 0.91$; $p < 0.01$).

767 **Fig. 6.** Comparison of the stratigraphic variations of (a) $C_{31}/(C_{29} + C_{31})$ ratio at Loma
768 Capiro, and (b) $C_{31}/(C_{29} + C_{31})$ ratio and (c) floral composition in Far East Asia
769 across the Cretaceous–Paleogence boundary. *Berggren et al. (1995); **Smit
770 (1982); ***Arenillas et al. (2004).

771

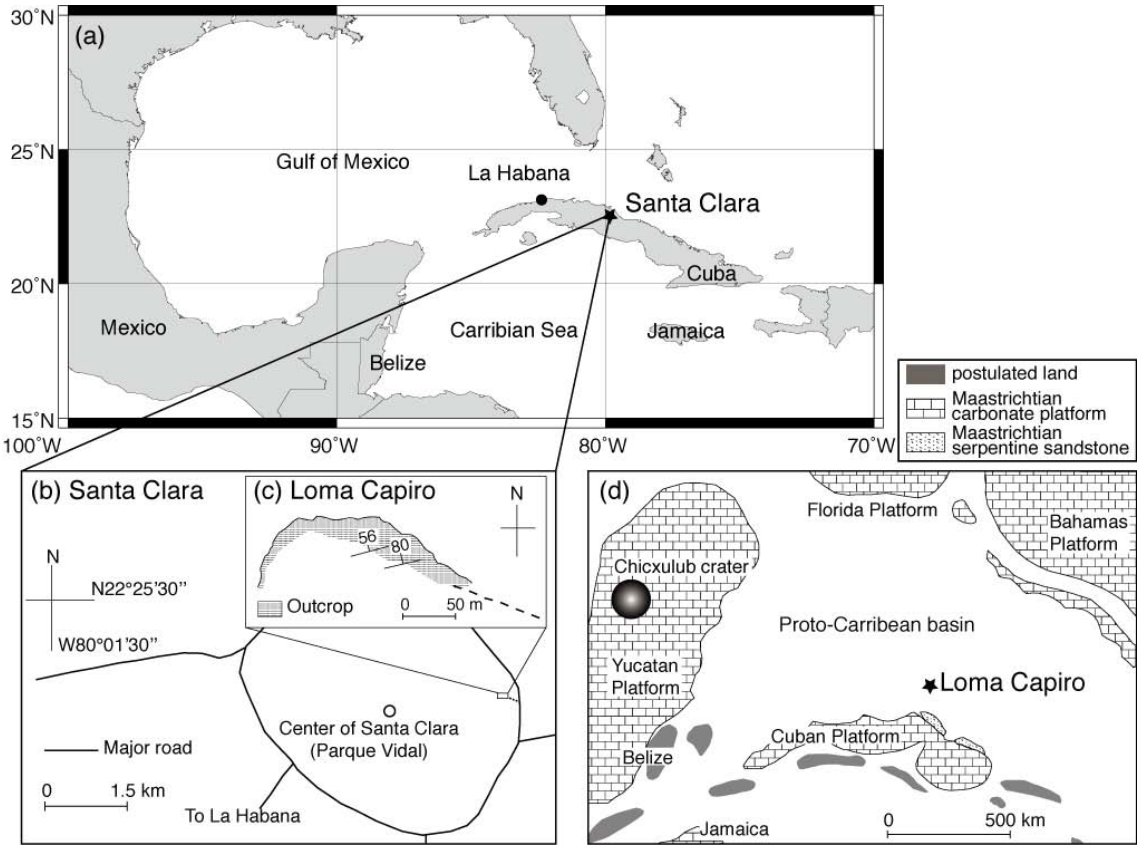

771

772

773 Fig. 1

774

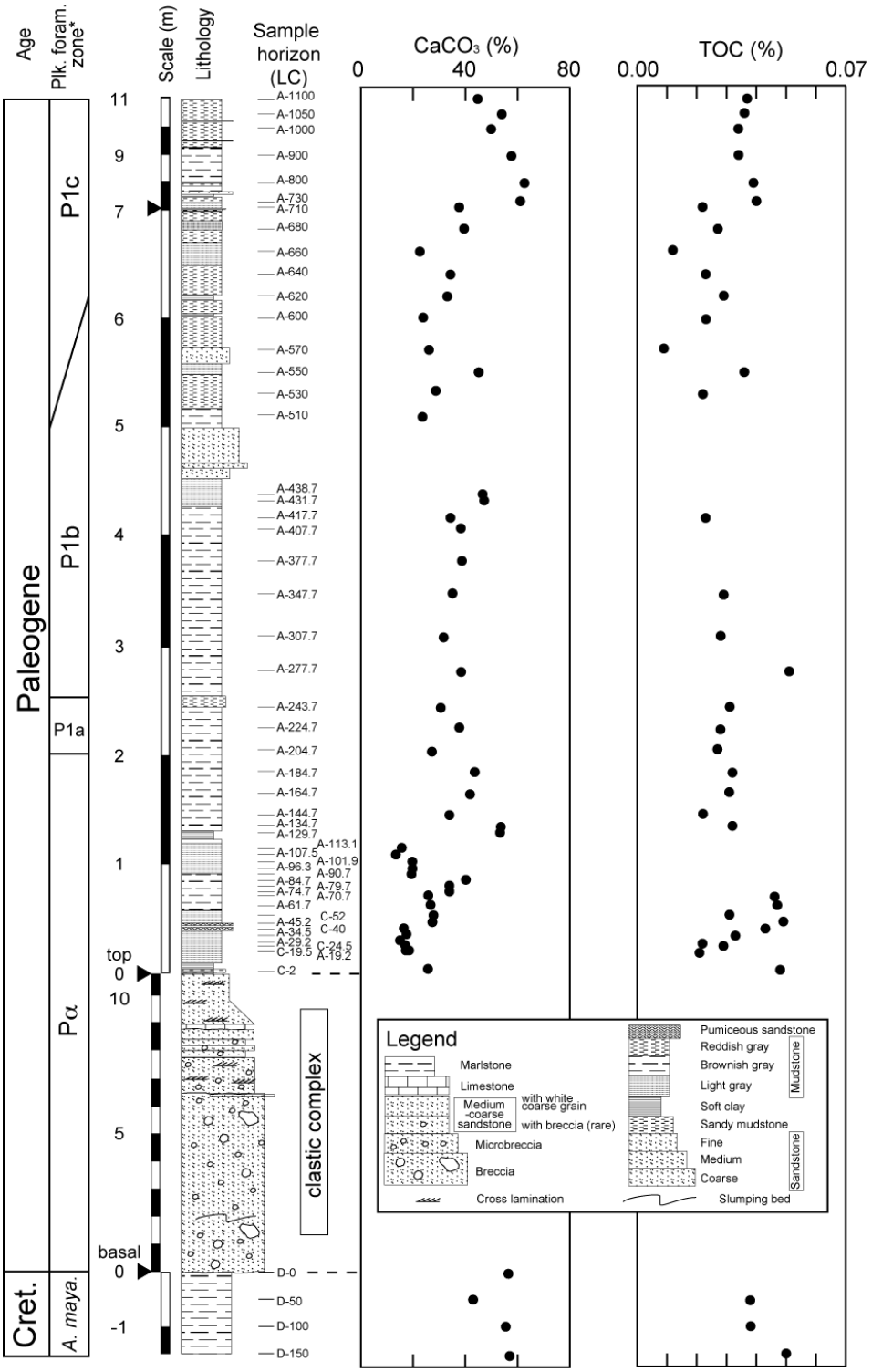
Age
Plk. foram. zone*
Scale (m)
Lithology
Sample horizon (LC)
CaCO3 (%)
TOC (%)
Paleogene
Cret.
P1c
P1b
P1a
Pα
A. maya.
clastic complex
top
basal
Legend
Marlstone
Limestone
Medium -coarse sandstone
with white coarse grain
with breccia (rare)
Microbreccia
Breccia
Cross lamination
Slumping bed
Pumiceous sandstone
Reddish gray
Brownish gray
Light gray
Soft clay
Sandy mudstone
Fine
Medium
Coarse
Mudstone
Sandstone

Fig. 2

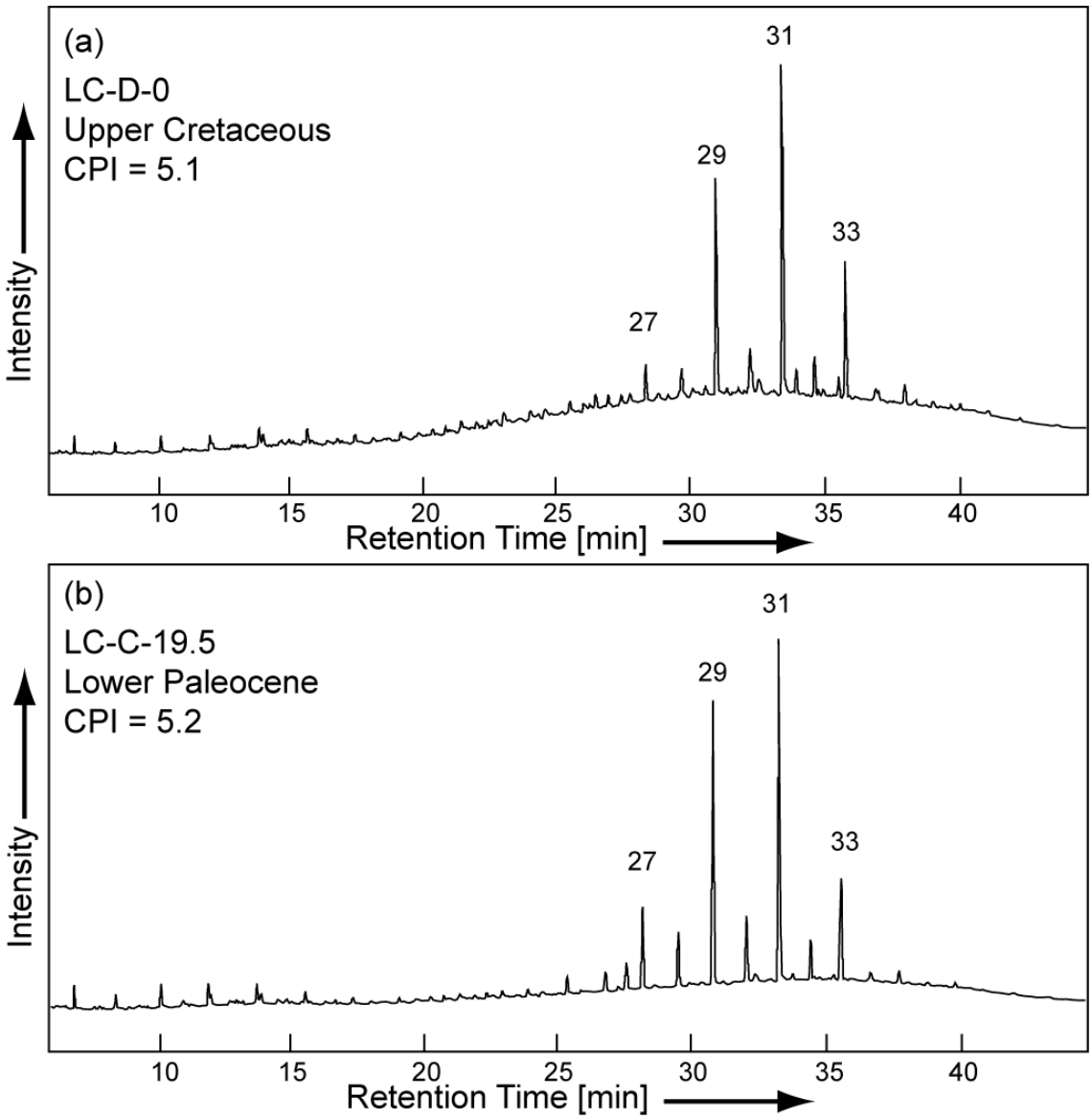

777

778

779 Fig. 3

780

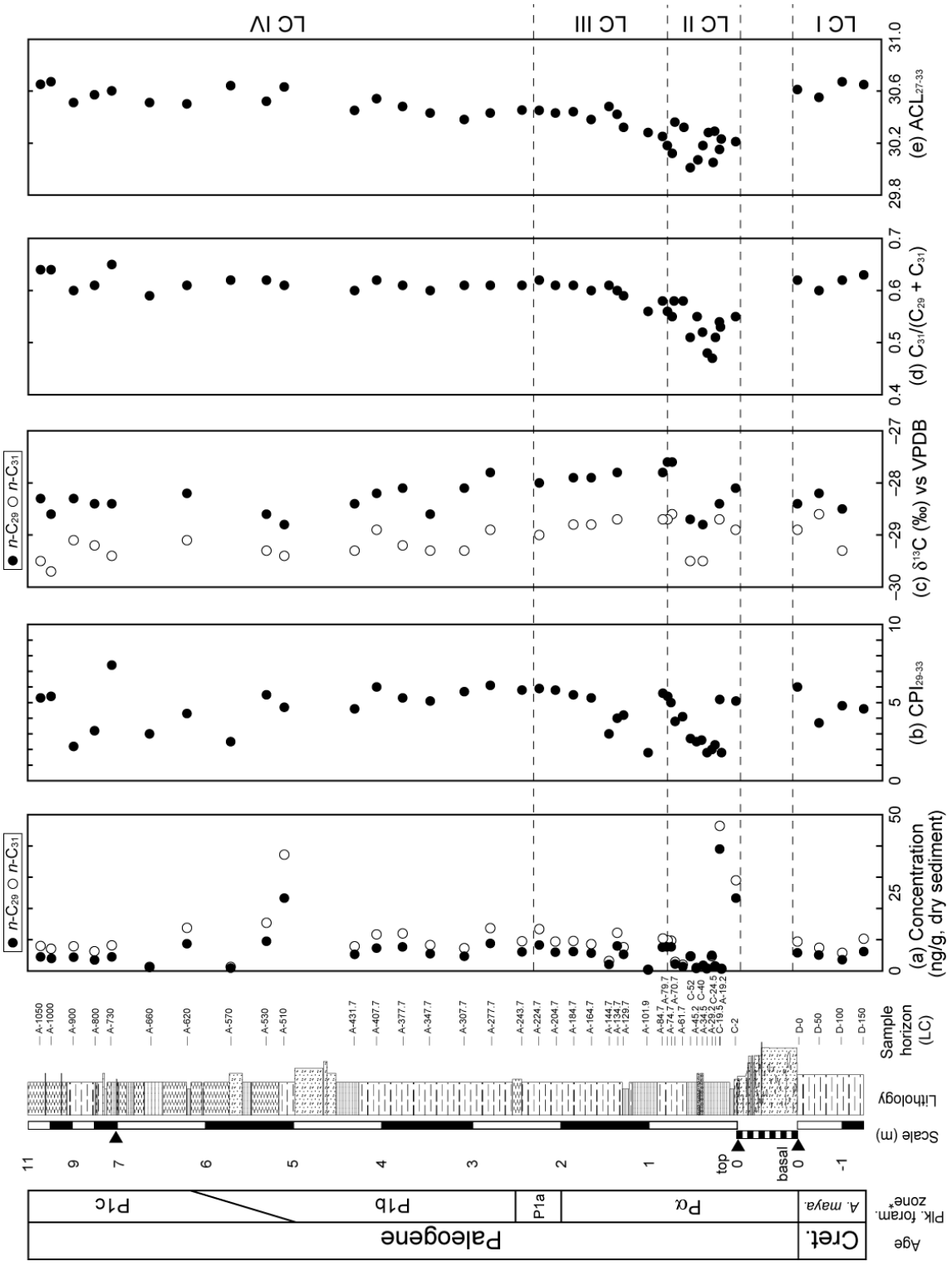
LC I
LC II
LC III
LC IV
(e) ACL27-33
(d) C31/(C29 + C31)
(c) δ13C (‰) vs VPDB
(b) CPI29-33
(a) Concentration (ng/g, dry sediment)
n-C29 ○ n-C31
Sample horizon (LC)
Lithology
Scale (m)
Age
Plk. foram. zone*
Cret.
Paleogene
A. mayaroensis
Pα
P1a
P1b
P1c
top
basal

Fig. 4

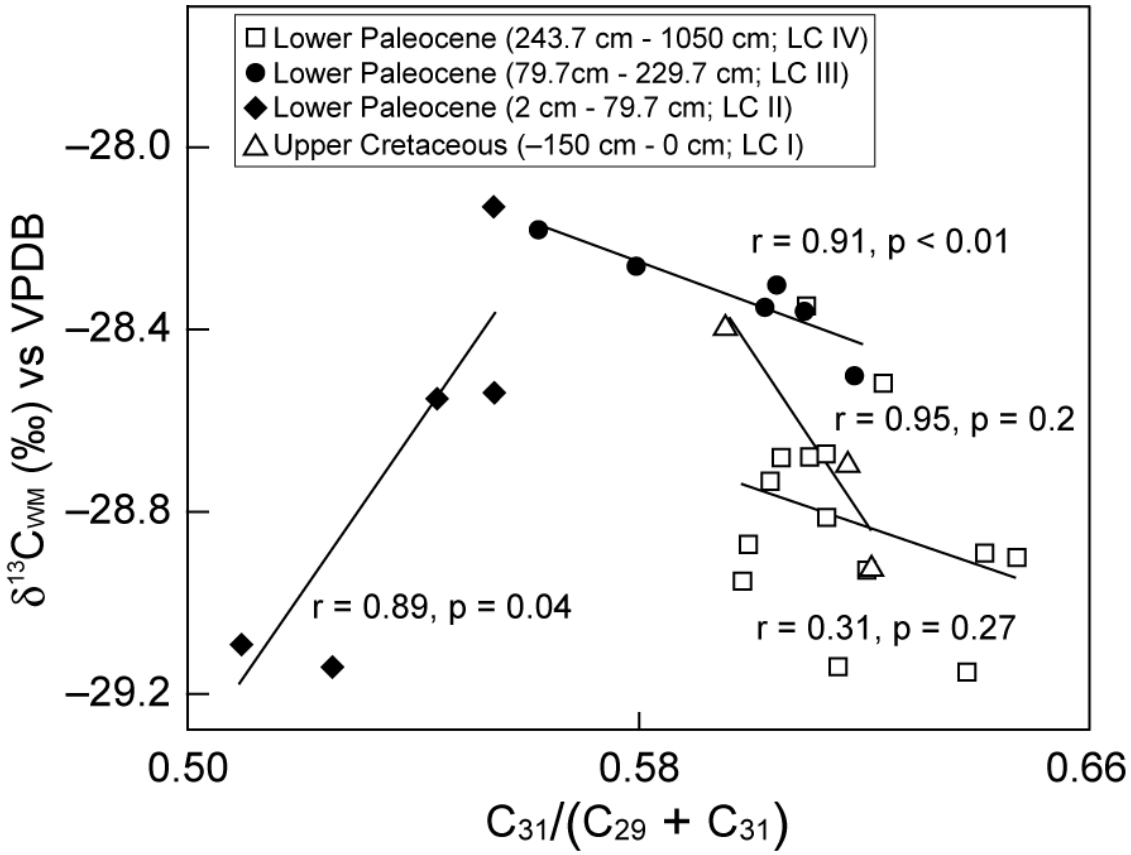
Lower Paleocene (243.7 cm - 1050 cm; LC IV)
Lower Paleocene (79.7cm - 229.7 cm; LC III)
Lower Paleocene (2 cm - 79.7 cm; LC II)
Upper Cretaceous (–150 cm - 0 cm; LC I)
r = 0.91, p < 0.01
r = 0.95, p = 0.2
r = 0.89, p = 0.04
r = 0.31, p = 0.27
–28.0
–28.4
–28.8
–29.2
0.50
0.58
0.66
δ13CWM (‰) vs VPDB
C31/(C29 + C31)

Fig. 5

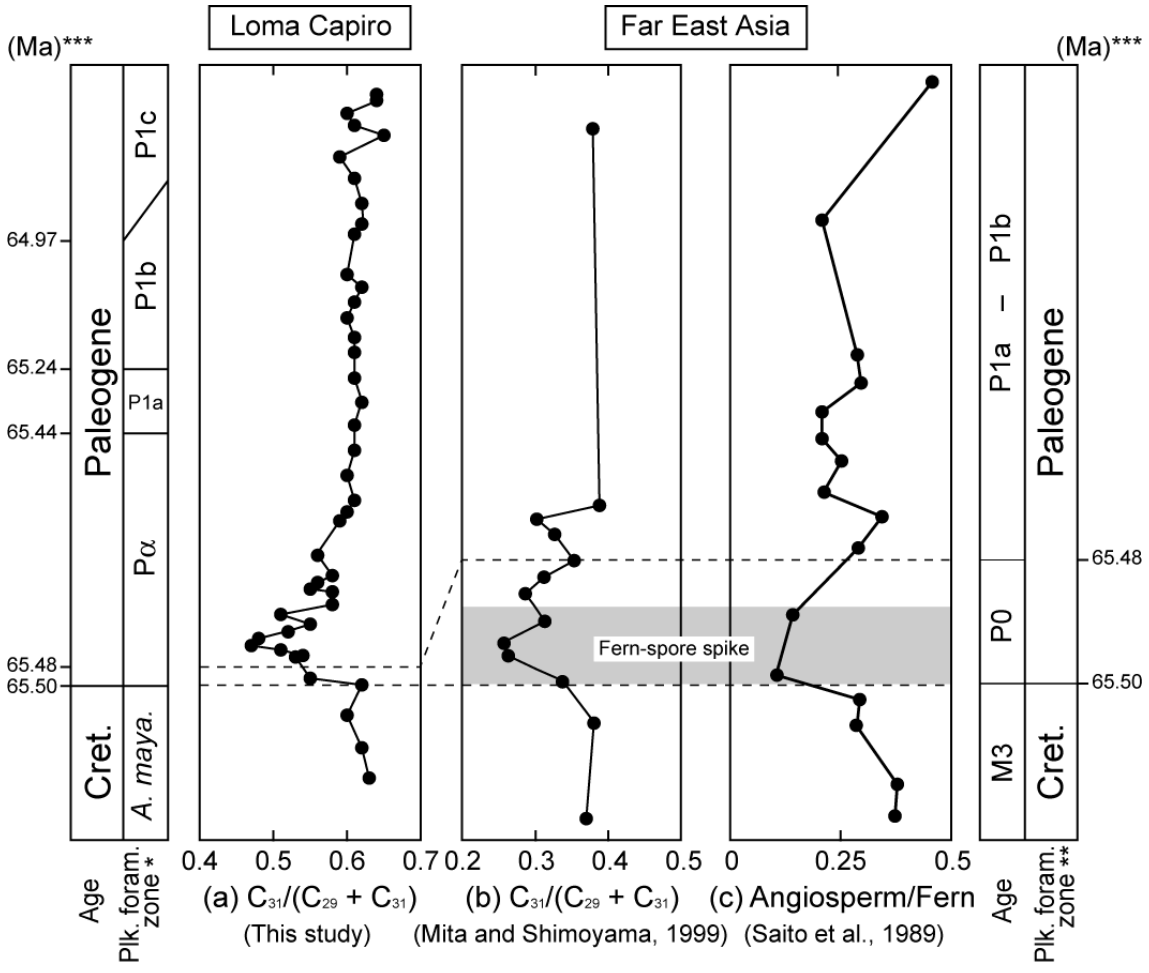
Loma Capiro
Far East Asia
(Ma)***
(Ma)***
Paleogene
Cret.
P1c
P1b
P1a
Pα
A. maya.
64.97
65.24
65.44
65.48
65.50
P1a – P1b
P0
M3
Paleogene
Cret.
65.48
65.50
Fern-spore spike
0.4 0.5 0.6 0.7
0.2 0.3 0.4 0.5
0 0.25 0.5
(a) C31/(C29 + C31)
(This study)
(b) C31/(C29 + C31)
(Mita and Shimoyama, 1999)
(c) Angiosperm/Fern
(Saito et al., 1989)
Age
Plk. foram. zone*
Age
Plk. foram. zone**

Fig. 6